

A high resolution spectroscopic atlas of M subdwarfs - Effective temperature and metallicity [★]

Rajpurohit, A. S.¹, Reyl  , C.¹, Allard, F.², Scholz, R.-D.³, Homeier D.², Schultheis, M.⁴, Bayo, A.^{5,6}

¹ Institut UTINAM, CNRS UMR 6213, Observatoire des Sciences de l'Univers THETA Franche-Comt  -Bourgogne, Universit   de Franche Comt  , Observatoire de Besan  on, BP 1615, 25010 Besan  on Cedex, France e-mail: arvind@obs-besancon.fr

² Centre de Recherche Astrophysique de Lyon, CNRS UMR 5574, Universit   de Lyon,   cole Normale Sup  rieure de Lyon, 46 all  e d'Italie, 69364 Lyon Cedex 07, France

³ Leibniz-Institut f  r Astrophysik Potsdam (AIP), An der Sternwarte 16, D-14482 Potsdam, Germany

⁴ Universit   de Nice Sophia-Antipolis, Observatoire de C  te d'Azur, Lagrange, CNRS UMR 7293, 06304 Nice Cedex 4, France

⁵ European Southern Observatory, Alonso de C  rdova 3107, Vitacura, Santiago, Chile

⁶ Max Planck Institut f  r Astronomie, Konigstuhl 17, 69117, Heidelberg, Germany

Received ...; accepted ...

ABSTRACT

Context. M subdwarfs are metal poor and cool stars. They are important probes of the old galactic populations. However, they remain elusive due to their low luminosity. Observational and modeling efforts are required to fully understand their physics and to investigate the effects of metallicity in their cool atmospheres.

Aims. We perform a detailed study of a sample of subdwarfs to determine their stellar parameters and constrain the state-of-the-art atmospheric models.

Methods. We present UVES/VLT high resolution spectra of three late-K subdwarfs and 18 M subdwarfs. Our atlas covers the optical region from 6400    up to the near infrared at 8900   . We show spectral details of cool atmospheres at very high resolution ($R \sim 40\,000$) and compare with synthetic spectra computed from the recent BT-Settl atmosphere models.

Results. Our comparison shows that molecular features (TiO, VO, CaH), and atomic features (Fe I, Ti I, Na I, K I) are well fitted by current models. We produce an effective temperature versus spectral type relation all over the subdwarf spectral sequence. Thanks to the high resolution of our spectra, we perform a detailed comparison of line profiles of individual elements such as Fe I, Ca II, Ti I, and are able to determine accurate metallicities of these stars. These determinations contribute to calibrate the relation between metallicity and molecular band strength indices from low-resolution spectra.

Conclusions. This work shows that the new generation of models are able to reproduce various spectral features of M subdwarfs. Working with these high resolution spectra allowed us to disentangle the atmospheric parameters (effective temperature, gravity, metallicity), which is not possible when using low resolution spectroscopy or photometry.

Key words. Stars: low-mass – subdwarfs – atmospheres

1. Introduction

M subdwarfs are metal poor, low-luminosity dwarfs. Very few are known and as a result the bottom of the main sequence is very poorly constrained for metal poor stars. The search for M subdwarfs is hampered not only by the fact that metal poor stars are rare and are intrinsically faint but also because late-type M subdwarfs do not show exceptionally red colours as ultracool-M dwarfs and brown dwarfs (L  pine et al. 2003a). Subdwarfs are typically very old (10 Gyr or more) belonging to the old Galactic populations: old disc, thick disc and spheroid, as shown by their spectroscopic features, kinematics properties and ages (Digby et al. 2003; L  pine et al. 2003a; Burgasser et al. 2003). As the low-mass subdwarfs, with their extremely long nuclear burning lifetimes, were presumably formed early in the Galaxy's history, they are important tracers of Galactic structure and chemical enrichment history. In addition, detailed studies of their complex spectral energy distributions give new insights on the

role of metallicity in the opacity structure, chemistry and evolution of cool atmospheres, and fundamental issues on spectral classification and temperature vs luminosity scales. Gizis (1997) proposed a first classification of M subdwarfs (sdM) and extreme subdwarfs (esdM) based on TiO and CaH band strengths in low resolution optical spectra. L  pine et al. (2007) have revised the adopted classification, and proposed a new classification for the most metal poor, the ultra subdwarfs (usdM). Jao et al. (2008) compared model grids with the optical spectra to characterize the M subdwarfs by three parameters: temperature, gravity, and metallicity and thus gave an alternative classification scheme of subdwarfs.

Spectroscopic studies of sdM at high resolution have proven to be a difficult task. In the low-temperature regime occupied by these stars, the optical spectrum is covered by a forest of molecular lines, hiding or blending most of the atomic lines used in spectral analysis. However, over the last decade, stellar atmosphere models of very low mass stars have made great progresses exploring metallicity effects (Allard et al. 2012, 2013). One of the most important recent improvement is the revision of the solar abundances (Asplund et al. 2009; Caffau et al. 2011).

[★] Based on observations made with the ESO Very Large Telescope at the Paranal Observatory under programme 087.D-0586A and 087.D-0586B

Rapid progress in the investigation of cool atmospheres is expected thanks to the advent of 8-meter class telescopes that allow high resolution spectroscopy of these faint targets. In high resolution spectra, access to weak lines allows us to determinate the metallicity disentangled from the other main parameters, gravity and effective temperature. The pressure changes affect equally all atmospheric parameters and therefore the various absorption bands. The determination of gravity from the pressure broadened wings can be expected to be much more accurate than comparing colour ratios from photometry or low resolution spectra. Thus it is necessary to achieve a very good fit in all important absorbers in order to determine atmospheric properties, because the chemical complexity of these atmospheres reacts sensibly to the major opacities. Descriptions of these stars therefore need validations by comparing with high resolution spectroscopic observations.

Measuring metallicities for M dwarfs is also challenging. Over the entire M dwarf sequence, the effective temperature ranges from about 4000 K to 2400 K (see e.g. Rajpurohit et al. 2013). With decreasing temperature, the spectra show increasingly abundant diatomic and triatomic molecules. In particular, the TiO and H₂O bands have complex and extensive absorption structures, creating a pseudo-continuum letting through only the strongest, often resonance, atomic lines. Woolf & Wallerstein (2005); Woolf et al. (2009) obtained metallicities from high resolution spectra by measuring equivalent widths of atomic lines in regions less dominated by molecular bands. Metallicities have also been obtained in binaries containing an M-type and a solar-type star from the much better understood spectra of the latter (Bonfils et al. 2005; Bean et al. 2006a,b). These results, together with the abundances obtained from high resolution spectra, are combined to calibrate metallicities using photometry or molecular indices (Bonfils et al. 2005; Woolf et al. 2009; Casagrande et al. 2008).

Metal poor stars are rare in the solar neighborhood and the current sample of local subdwarfs is very limited. High resolution spectra of M dwarfs were shown by Tinney & Reid (1998) on the full optical range but such observations are not available for the M subdwarfs on the whole temperature sequence. In this paper we present the first high resolution optical atlas of stars covering the whole sdM, esdM and usdM sequence. It consists of 2/11 sdK/sdM, 1/5 esdK/esdM, and 2 usdM observed with UVES at VLT. Using the most recent PHOENIX BT-Settl stellar atmosphere models we have performed a detailed comparison with our observed spectra. In this study we compare the models to the high resolution spectra of sdM at subsolar metallicities and we assign effective temperatures. We derive metallicities based on the best fit of synthetic spectra to the observed spectra and perform a detailed comparison of lines profile of individual elements such as Fe I, Ca II, Ti I, Na.

High resolution spectroscopic observations are described in Section 2 and the model atmospheres used for comparison are presented in Section 3. The comparison between observed and synthetic spectra and the derived stellar parameters are given in Section 4. In Section 5, we present effective temperature versus colours and spectral type relations, and metallicity calibrations. The conclusion is in Section 6.

2. A high resolution spectral atlas of M subdwarfs

High resolution spectroscopy is a very important tool to understand the physics of stars. The identification of atomic and molecular absorptions features in the spectra of M subdwarfs is important as they can be used to constrain the main stellar parameters T_{eff} , $\log g$, [Fe/H]. The determination of gravity from

its effect on the pressure dependent wings of the saturated atomic absorption lines (predominantly of the alkali elements) is expected to be much more accurate than comparing colour ratios from low resolution spectra (Reiners et al. 2007).

We present a high resolution spectral atlas of 21 very low mass objects that we selected to cover the entire M subdwarf spectral range, including 6 extreme and 2 ultra subdwarfs. The name, spectral type, and near-infrared photometry of these objects are given in Table 1. The photometry are taken from the Two Micron All Sky Survey (2MASS, Skrutskie et al. 2006). The spectral types and spectral indices are found in the literature.

2.1. Observation and data reduction

The observations were carried out in visitor mode during April and September 2011 with the optical spectrometer UVES (Dekker et al. 2000) on the Very Large Telescope (VLT) at the European Southern Observatory (ESO) in Paranal, Chile. UVES was operated in dichroic mode using red arm with non-standard setting centered at 830 nm. This setting covers the wavelength range 6400 Å–9000 Å, which contains various atomic lines like Fe I, Ti I, K II, Na I and Ca II and is very useful for the spectral synthesis analysis. Between the two CCDs of the red arm, the spectra have a gap from 8200 Å to 8370 Å. The Na doublet at 8190 Å lies just blue ward of the gap. The spectra were taken with a slit width of 1.0'' yielding a nominal resolving power of $R = 40000$. The signal to noise ratio varies over the wavelength region according to the object's spectral energy distribution and detector efficiency. It reaches 30 to more than 100 depending on the magnitude of the targets in most of the spectral region so that the dense molecular and atomic absorption features are well discernible from noise. Data were reduced using the software called Reflex for UVES data which runs standard ESO pipelines modules.

The spectra are shown in Fig. 1 for a representative sample along the sdM sequence, and in Fig. 2 for the esdM and usdM targets. The spectra shown have not been corrected for terrestrial absorption by O₃ and H₂O. The O₃ features are quite regular and straightforward to disentangle from features in the stars themselves. This is not true for H₂O absorption, which is complex and irregular (Tinney & Reid 1998). We therefore show in the upper panels the spectrum of the reference star EG 21 where telluric absorptions appear. The main molecular and atomic features expected in the M subdwarfs are labelled in Fig.1 and Fig. 2.

2.2. Molecular features

The optical spectra are dominated by molecular absorption bands from metal oxide species such as titanium oxide (TiO), vanadium oxide (VO), hydrides like CaH and H₂O. They are the most important opacity sources. However, due to the low metallicity of subdwarfs, they are TiO depleted. The primary effects are the strengthening of hydride bands and collision induced absorption (CIA) by H₂, and the broadening of atomic lines (Allard et al. 1997). Unlike TiO, which produces distinctive band heads degraded on the red, VO produces more diffuse absorption. CaH hydride bands are important opacity sources but decrease in relative strength and become saturated with decreasing temperature.

Table 1: Spectral types, near-infrared photometry, and spectral indices of our sample. The photometry and coordinates are taken from 2MASS, at epochs between 1997 and 2001. References are given for spectral types first and spectral indices next.

Name	α	δ	SpT	J	H	K_s	TiO5	CaH2	CaH3	Ref.
LHS 72	23 43 13.5	-24 09 50	sdK4	9.61	9.04	8.82	—	—	—	a,—
LHS 73	23 43 16.6	-24 11 14	sdK7	10.11	9.59	9.37	0.960	0.847	0.901	b,b
G 18-37	22 14 55.5	+05 42 37	esdK7	12.72	12.20	12.02	—	—	—	c,—
APMPM J2126-4454	21 26 23.9	-44 53 34	sdM0	12.65	12.11	11.92	—	—	—	d,—
LHS 300	11 11 13.8	-41 05 33	sdM0	10.48	10.01	9.80	1.031	0.886	0.943	e,e
LHS 401	15 39 39.1	-55 09 10	sdM0.5	10.15	9.60	9.41	0.997	0.911	0.958	e,e
LHS 158	02 42 02.8	-44 30 59	sdM1	10.43	9.94	9.73	0.732	0.639	0.829	e,e
LHS 320	12 02 33.7	+08 25 51	sdM2	10.74	10.18	9.99	0.620	0.512	0.751	f,f
LHS 406	15 43 18.4	-20 15 31	sdM2	9.78	9.23	9.02	0.686	0.576	0.789	e,e
LHS 161	02 52 45.6	+01 55 50	esdM2	11.71	11.20	11.00	0.889	0.689	0.817	f,e
LP 771-87	03 07 34.0	-17 36 38	usdM2	15.60	15.29	14.90	—	—	—	g,—
LHS 541	23 17 06.0	-13 50 53	sdM3	13.03	12.56	12.41	0.730	0.467	0.664	h,h
LHS 272	09 43 46.3	-17 47 07	sdM3	9.62	9.12	8.87	0.678	0.441	0.669	f,f
LP 707-15	01 09 54.1	-10 12 13	esdM3	12.94	12.40	12.16	—	—	—	c,—
LSR 1755+1648	17 55 32.8	+16 48 59	sdM3.5	11.35	10.89	10.63	0.486	0.419	0.664	i,i
LHS 375	14 31 38.3	-25 25 33	esdM4	12.15	11.67	11.51	0.829	0.372	0.547	f,f
LHS 1032	00 11 00.8	+04 20 25	usdM4.5	14.34	13.81	13.76	0.944	0.374	0.514	j,j
SSSPM J0500-5406	05 00 15.8	-54 06 27	esdM6.5	14.44	14.12	13.97	0.755	0.220	0.331	h,h
LHS 377	14 39 00.3	+18 39 39	sdM7	13.19	12.73	12.48	0.232	0.205	0.396	f,f
APMPM J0559-2903	05 58 58.9	-29 03 27	esdM7	14.89	14.45	14.46	0.600	0.210	0.320	l,l
SSSPM J1013-1356	10 13 07.3	-13 56 20	sdM9.5	14.62	14.38	14.40	0.208	0.116	0.200	m,m

(a) Rodgers & Eggen (1974); Bidelman (1985) – (b) Reylé et al. (2006) – (c) S. Lépine, private communication – (d) Scholz et al. (2002) – (e) Jao et al. (2008) – (f) Gizis (1997) – (g) Kirkpatrick et al. (2010) – (h) Dawson & De Robertis (2000) – (i) Lépine et al. (2003b) – (j) Lépine et al. (2007) – (k) Burgasser & Kirkpatrick (2006) – (l) Schweitzer et al. (1999) – (m) Scholz et al. (2004)

2.3. Atomic lines

All the observed M subdwarfs show strong alkali lines in the observed wavelength range. They are massively pressure broadened as expected from their high gravity surface. Atomic features such as Ca II, K I, Rb I, Na I, Ti I, Mg I are visible throughout the sequence and their lines are prominent in almost all of the spectra. However, in regions where strong atmospheric absorption is present, it is not easy to measure the intensities of these lines.

The Na I lines at 8183 Å and 8194 Å are clearly visible in all the observed spectra and become broadened as one goes from hotter to cooler M subdwarfs. In our setting they appear just at the red end of the lower chip of the blue arm. The K I lines are very narrow for early type but become very wide and smooth in late type subdwarfs. The K I resonance lines at 7665 Å and 7698 Å govern the spectral shape of cool subdwarfs spectra. The equivalent width of these K I lines are of several hundred Å. The ionized Ca II triplet lines at 8498 Å, 8542 Å, 8662 Å are very strong in all the observed spectra. Their detailed study by Mallik (1997) shows that their strengths depend on stellar parameters like luminosity, temperature and metallicity. They are ideal candidates to study their sensitivity to various stellar parameters in cool stars. Although the Ca II triplet lines have lower levels populated radiatively and are not collision controlled, they have been identified as very good luminosity probes Mallik (1997). They are relatively free from blends and are not much contaminated by telluric lines. On the contrary, the Na I lines at 8183 Å and 8195 Å, which have also been used as luminosity probes in cool stars, have several atmospheric absorption lines in their vicinity (Alloin & Bica 1989; Zhou 1991).

3. Model atmospheres

In this study, we use the most recent BT-Settl models partially published in a review by Allard et al. (2012). These atmosphere models are computed with the PHOENIX multi-purpose atmosphere code version 15.5 (Hauschildt et al. 1997; Allard et al. 2001) solving the radiative transfer in 1D spherical symmetry, with the classical assumptions: hydrostatic equilibrium, convection using the mixing length theory, chemical equilibrium, and a sampling treatment of the opacities. The models use a mixing length as derived by the radiation hydrodynamic simulations of Ludwig et al. (2002, 2006); Freytag et al. (2012).

Relative to previous models by Allard et al. (2001), the current version of the BT-Settl model atmosphere is using the BT2 water vapor line list computed by Barber et al. (2006), TiO, VO, CaH line lists by Plez (1998), MgH by Weck et al. (2003); Skory et al. (2003), FeH and CrH by Dulick et al. (2003); Chowdhury et al. (2006), CO₂ by Tashkun et al. (2004), H₂ CIA by Borysow et al. (2001); Abel et al. (2011), and CO by Goorvitch & Chackerian (1994a,b), to mention the most important. We are also including the H₂-He CIA from Borysow & Frommhold (1989); Borysow et al. (1997), H₂-H from Gustafsson et al. (2003) and H-He (at least in the most recent models) from the Gustafsson & Frommhold (2001). Detailed profiles for the alkali lines are also used (Allard et al. 2007). The reference solar elemental abundances used in this version of the BT-Settl models are those measured by Caffau et al. (2011).

In general, the Unsold (1968) approximation is used, with the general exception of Na I, Si I, Ca I, Fe I, where we instead use the respective correction factors found by Gustafsson et al. (2008) for the atomic damping constants with a correction factor to the widths of 2.5 for the non-hydrogenic atoms (Valenti & Piskunov 1996). More accurate broadening data for neutral hydrogen collisions by Barklem et al. (2000) have been

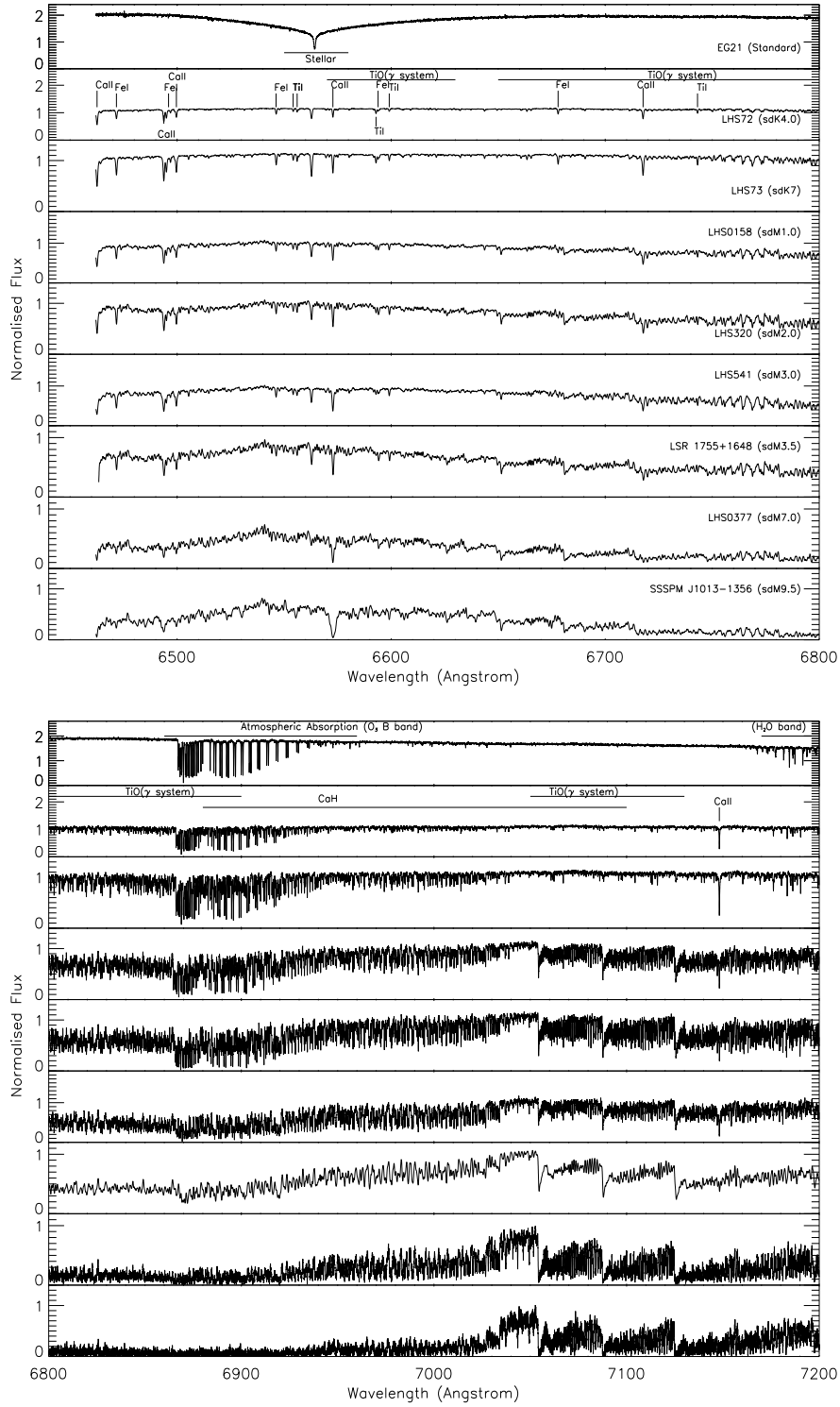


Fig. 1: UVES spectra over the sdM spectral sequence. The spectra are scaled to normalize the average flux to unity. The spectrum of the standard star EG 21 shows the location of telluric atmospheric features.

included for several important atomic transitions such as the alkali, CaI and CaII resonance lines. For molecular lines, we have adopted average values (e. g. $\langle \gamma_6^{HIT}(T_0, P_0^1) \rangle_{H_2O} = 0.08 P_{\text{gas}} [\text{cm}^{-1} \text{atm}^{-1}]$ for water vapor lines) from the HITRAN database (Rothman et al. 2009), which are scaled to the local gas

pressure and temperature

$$\gamma_6(T) = \langle \gamma_6^{HIT}(T_0, P_0) \rangle \left(\frac{296 \text{ K}}{T} \right)^{0.5} \left(\frac{P}{1 \text{ atm}} \right), \quad (1)$$

with a single temperature exponent of 0.5, to be compared to values ranging mainly from 0.3 to 0.6 for water transitions studied by Gamache et al. (1996). The HITRAN database gives widths

¹ Standard temperature 296 K and pressure 1 atm

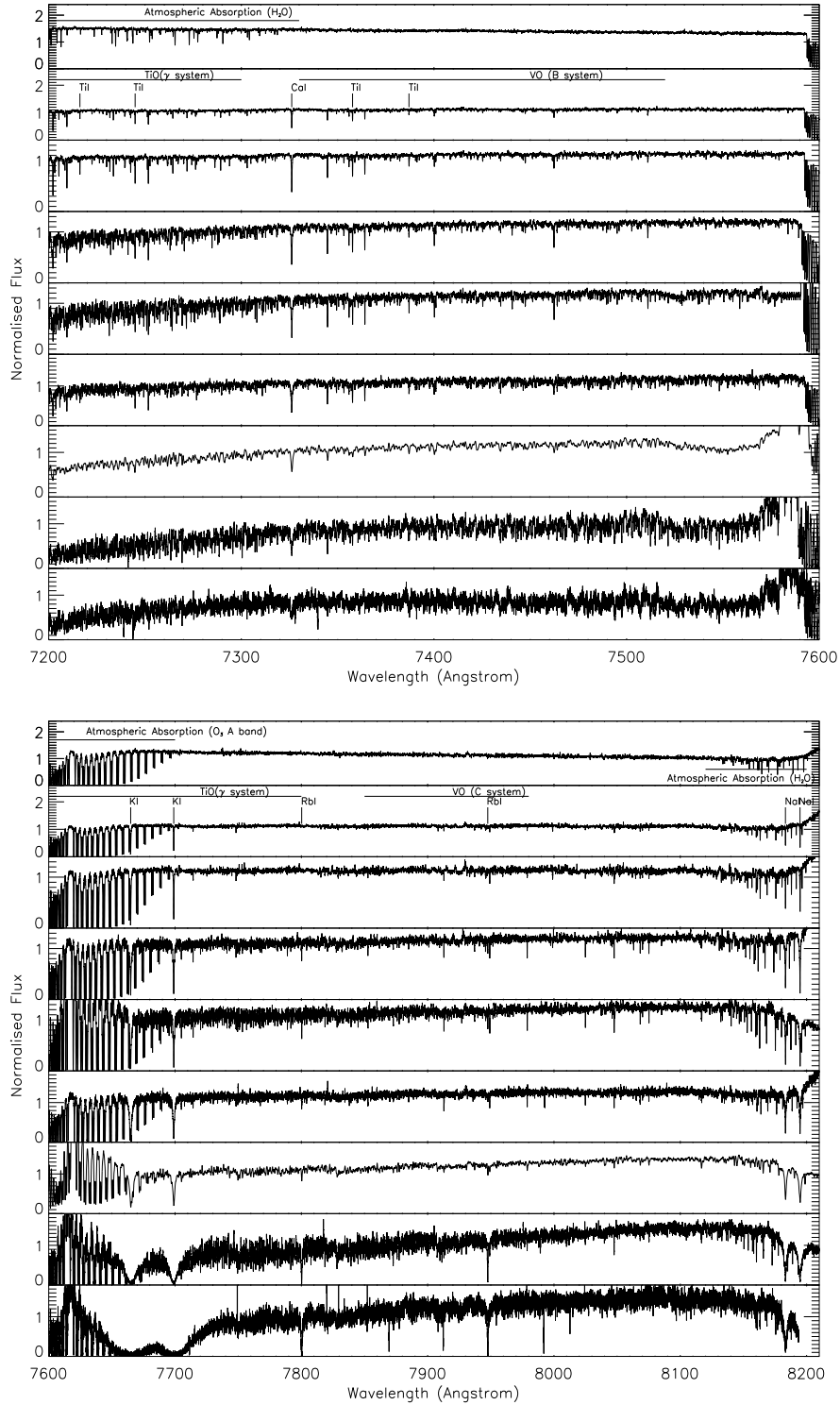


Fig. 1: Continued.

for broadening in air, but Bailey & Kedziora-Chudczer (2012) find that these agree in general within 10–20% with those for broadening by a solar composition hydrogen-helium mixture.

The BT-Settl grid extends from $T_{\text{eff}} = 300$ to 7000 K at a step of 100 K, $\log g = 2.5$ to 5.5 at a step of 0.5 and $[M/H] = -2.5$ to 0.0 at a step of 0.5 accounting for alpha element enrichment. The alpha enhancement is taken as $[\alpha/\text{Fe}] = -0.4 \times [\text{Fe}/\text{H}]$ for $0 > [\text{Fe}/\text{H}] > -1$ and 0.4 for metallicities < -1.0 which is also consis-

tent with the choice of Gustafsson et al. (2008). These different prescriptions for alpha enhancement are rough estimates for the old thin disc and thick disc, respectively (see e.g. Neves et al. 2009, for a discussion on the abundance trends relative to Fe).

We linearly interpolated the grid at every 0.1 dex in $\log g$ and metallicity. For more detail of BT-Settl model atmosphere see Allard et al. (2012, 2013); Rajpurohit et al. (2012). The syn-

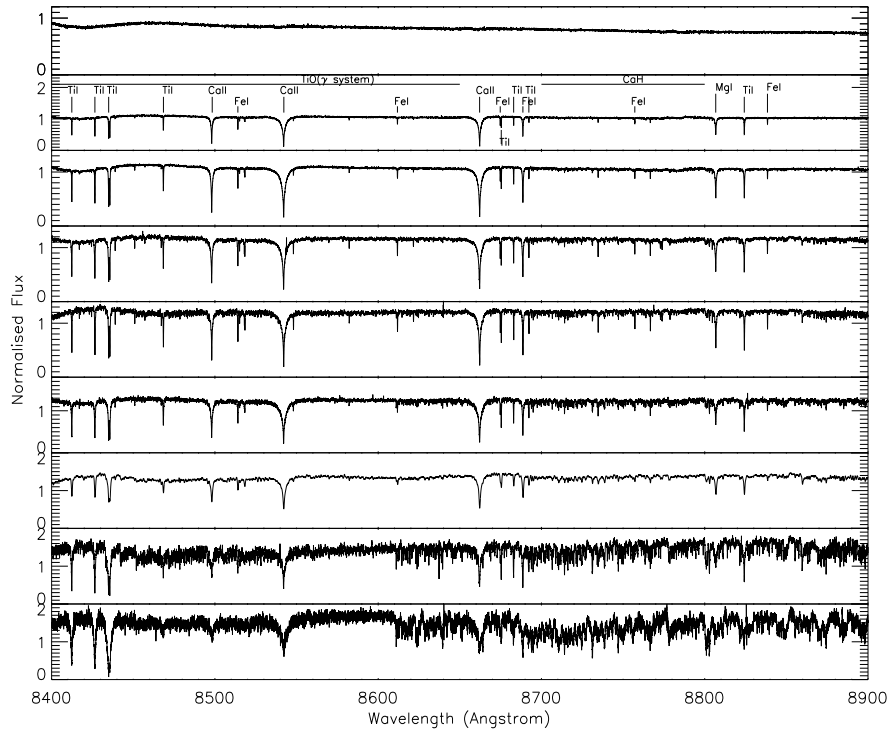


Fig. 1: Continued.

thetic colours and spectra are distributed with a resolution of around $R = 100000$ via the PHOENIX web simulator².

Fig. 3 shows BT-Settl synthetic spectra varying T_{eff} and $[M/H]$. Oxide bands that dominate in M dwarfs spectra are weaker in the subdwarfs where the hydride bands dominate (Jao et al. 2008). They have complex and extensive band structures leaving no window for the true continuum and creating pseudo continuum that only lets through the strongest, often resonance atomic lines (Allard 1990; Allard & Hauschildt 1995). However because of the lower metallicity of subdwarfs, the TiO bands are less strong, and the pseudo-continuum is brighter. This increases the contrast to the other opacities such as hydride bands and atomic lines which feel the higher pressures of the deeper layers where they emerge from. We see therefore these molecular bands with more details and under more extreme gas pressure conditions than for M dwarfs.

Although the models are computed for different $[M/H]$ values, in the following we use $[Fe/H]$ everywhere. Indeed we use only the iron lines for the metallicity determinations so that we in fact determine a $[Fe/H]$ value.

4. Comparison with model atmospheres

We perform a comparison between observed and synthetic spectra computed from the BT Settl model to derive the physical parameters of our sample. Furthermore, the comparison with observed spectra is very crucial to reveal the inaccuracy or incompleteness of the opacities used in the model. Fig. 4 and 5 shows the comparison of the best fit model for an sdM1 and an usdM4.5 star.

4.1. Molecular bands

The spectra are in good agreement, and able to reproduce the specific strengths of the TiO band heads at 6600 Å, 6700 Å, 7050 Å, 7680 Å, 8859 Å, and VO bands at 7000 Å, 7430 Å, 7852 Å. The excellent match between models and observations over entire subdwarf sequence shows that the high frequency pattern visible at this spectral resolution is the structure of the absorption band and not noise.

4.2. Atomic lines

The models predict rather well the shape of the Na I doublet at 8194 Å and 8183 Å but its strength is not very well fitted. In the sdM3.0 and later and in esdM, the observed lines are broader and shallower than those predicted by the models.

The qualitative behaviour of the K I doublet at 7665 Å and 7698 Å is well reproduced by the models, especially the strong pressure broadening wings in the early sdM and esdM. In the sdM0, the cores of the observed K I lines are still visible as relatively narrow absorption minima embedded in wings extending a few tens to hundred Å. This broader absorption component becomes saturated in sdM7 spectrum. The models also show this effect but are not able to reproduce it perfectly. This could be an indication (i) that the models do not yet produce correct densities of the neutral alkali metals in the uppermost part of the atmosphere, since the central parts of the lines form in the highest layers of the atmosphere, especially in the early sdM and esdM where alkali metals are not depleted strongly (Johnas et al. 2007), or (ii) that the depth of atomic lines can only be reproduced when accounting for a magnetic field and Zeeman broadening (Deen 2013).

The models reproduce the strength and wings of Ca II triplet lines at 8498 Å, 8542 Å, 8662 Å very well. We also have a good

² <http://phoenix.ens-lyon.fr/simulator>

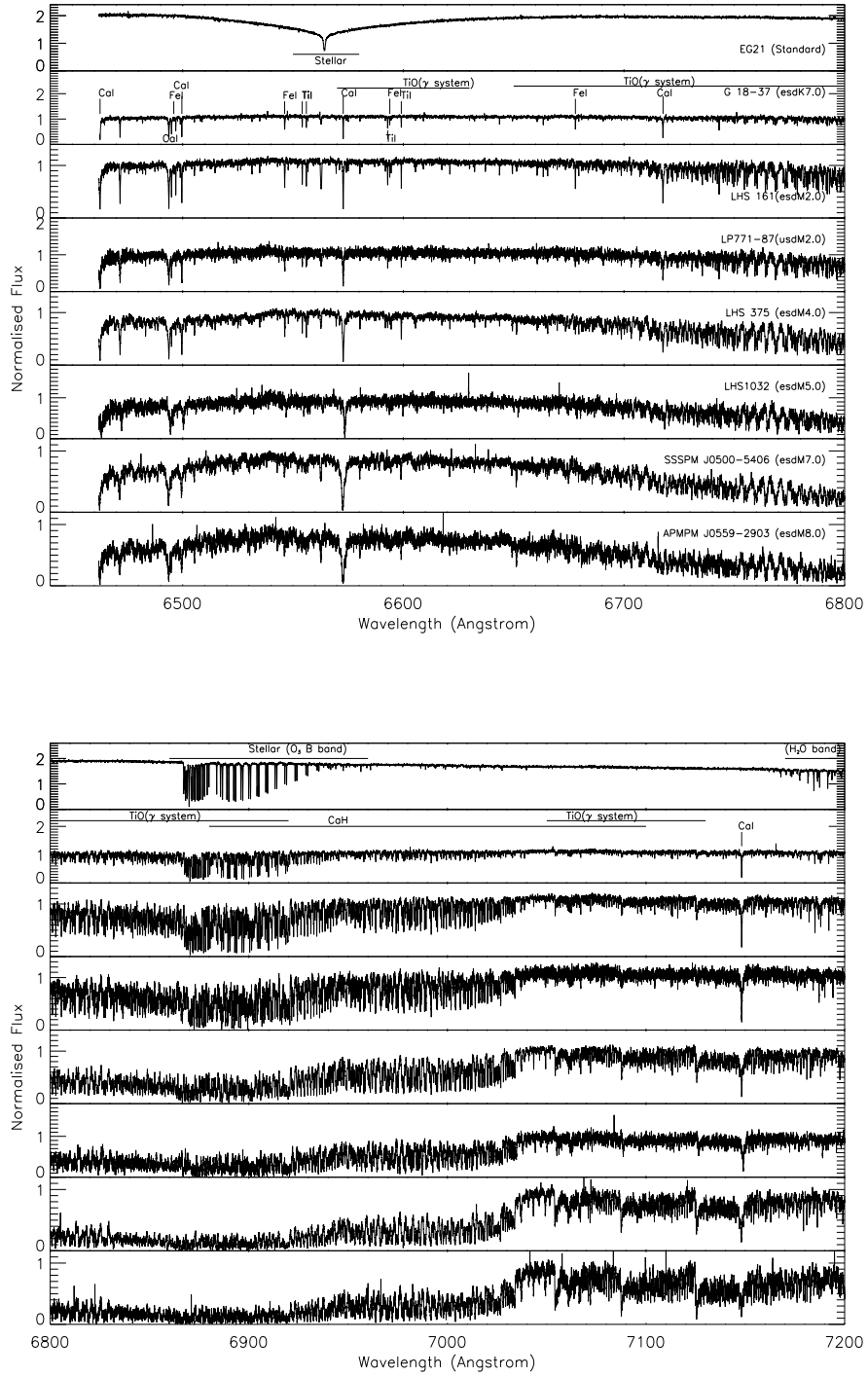


Fig. 2: Same as Fig. 1 for esdM and usdM stars.

fit to the Ti I lines. They are located between 8400 Å to 9700 Å and belong to low energy transitions that appear to be visible in such cool atmospheres (see also Reiners & Basri 2006).

Absorption lines of Rb appear in spectra later than sdM7.0. They become stronger and wider towards lower temperature. Given the fact that they are embedded in pseudo-continua that are not always a good fit to the data, the behavior of the two

Rb lines at 7800 Å and 7948 Å is very well reproduced by the models.

4.3. Stellar parameters determination

The analysis using synthetic spectra requires the specification of several input parameters: effective temperature, surface gravity and the overall metallicity compared to Sun. We first convolve

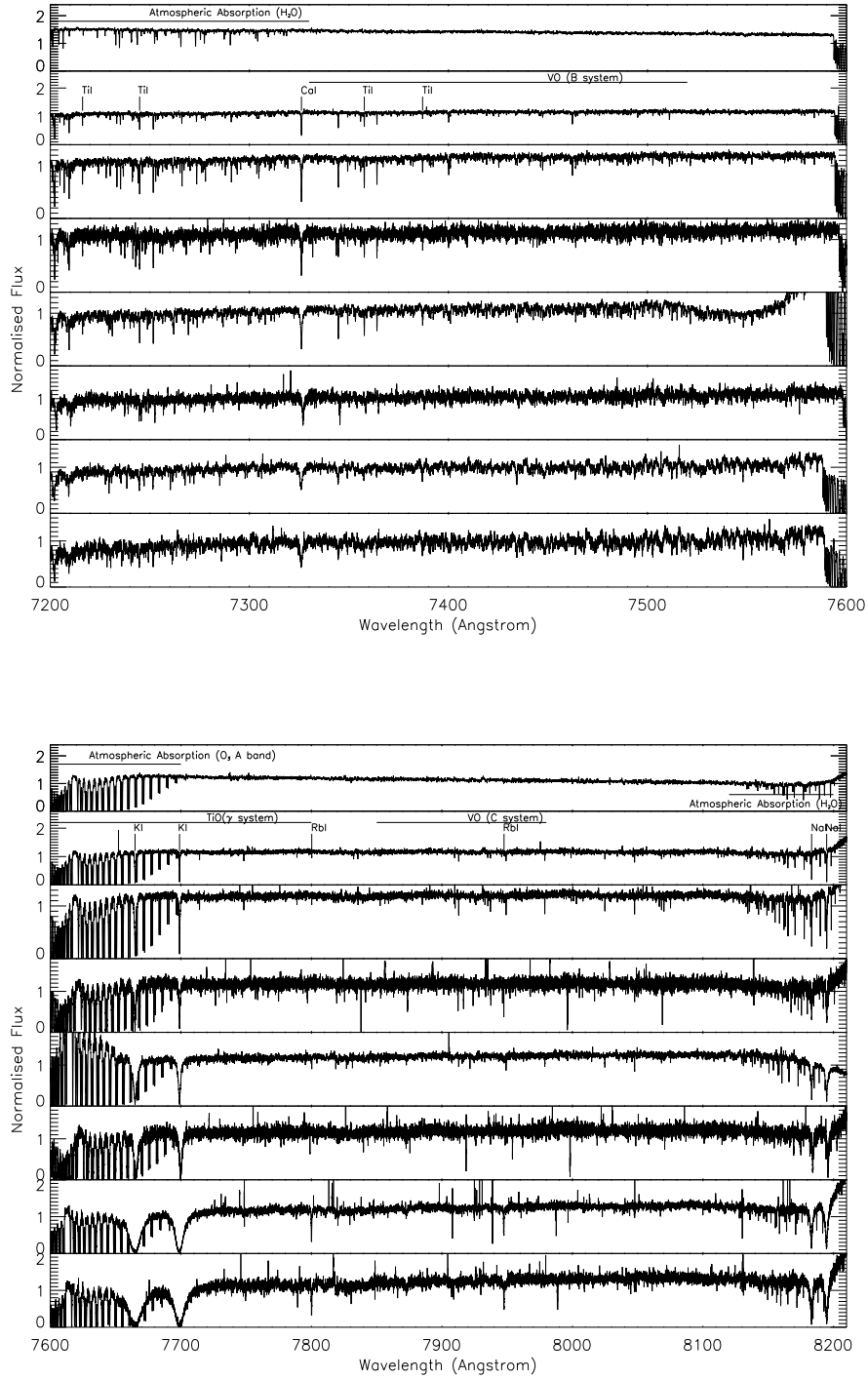


Fig. 2: Continued.

the synthetic spectrum with a Gaussian kernel at the observed resolution and then interpolate the outcome with the observation. We perform a χ^2 fitting between the grid of synthetic spectra and observed spectra in the wavelength range 6400 Å to 8900 Å as shown by Önehag et al. (2012). We have excluded the spectral region between 6860 to 6960 Å, 7550 to 7650 Å, and 8200 to 8430 Å, due to presence of atmospheric absorption. We let all the stellar parameters (T_{eff} , $[\text{Fe}/\text{H}]$, $\log g$) go free.

The minimum χ^2 value gives the best fit parameters and their error bars are derived by allowing a 5 % deviation of the χ^2 value from its minimum value. The acceptable parameters are finally inspected by comparing it with the observed spectra.

The TiO system at 6600 Å, 6700 Å and 7100 Å is highly sensitive to T_{eff} (increasing in strength with decreasing T_{eff}) and rather insensitive to variation in gravity. At a given T_{eff} , the band strengths change only slightly even for a large 0.5 change in

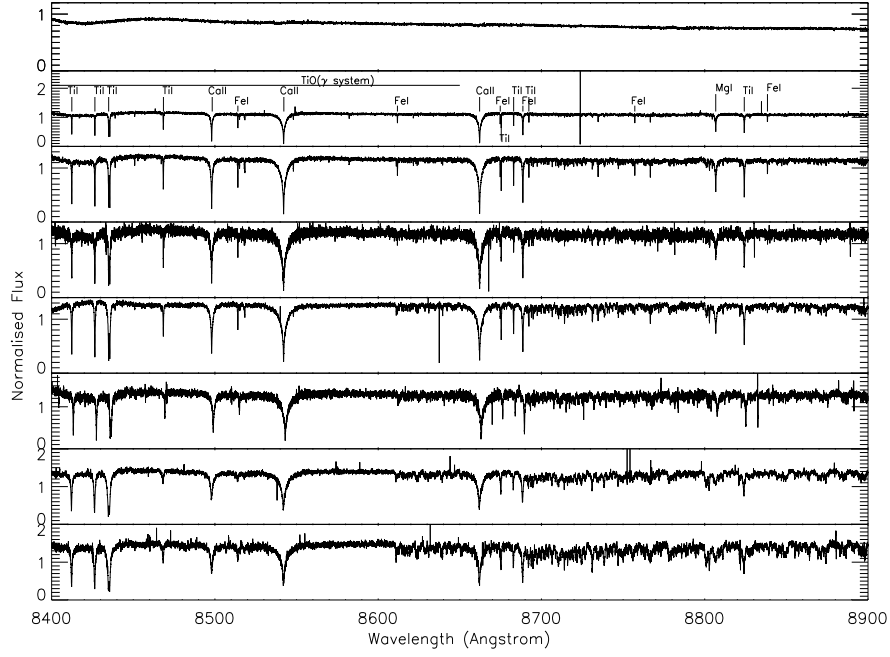


Fig. 2: Continued.

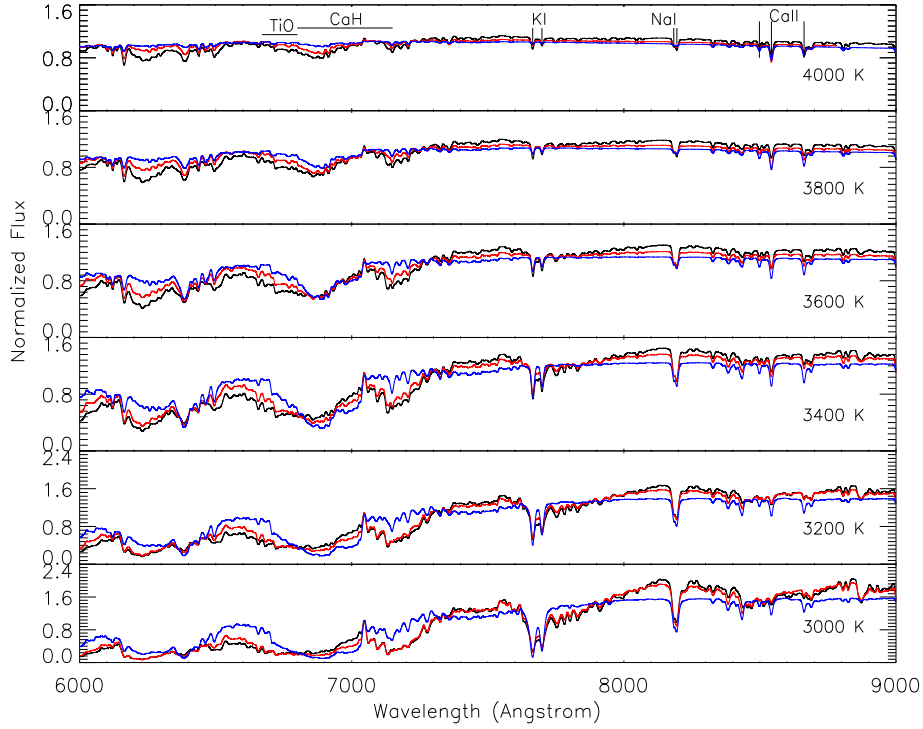


Fig. 3: BT-Settl synthetic spectra from 4000 K to 3000 K. The black, red, and blue lines represent $[M/H] = 0.0$, -1.0 , and -2.0 , respectively.

gravity (in the $\log g = 4.5$ - 5.5 range expected for low-mass stars). At a given gravity, however, they vary significantly over only 100 K change in T_{eff} .

The surface gravity determination is checked on the width of gravity sensitive atomic lines such as K I and Na I doublets (see Fig. 6) as well as relative strength of metal hydride bands such as CaH. The K I doublet at 7665 Å, 7699 Å and Na I lines at 8183

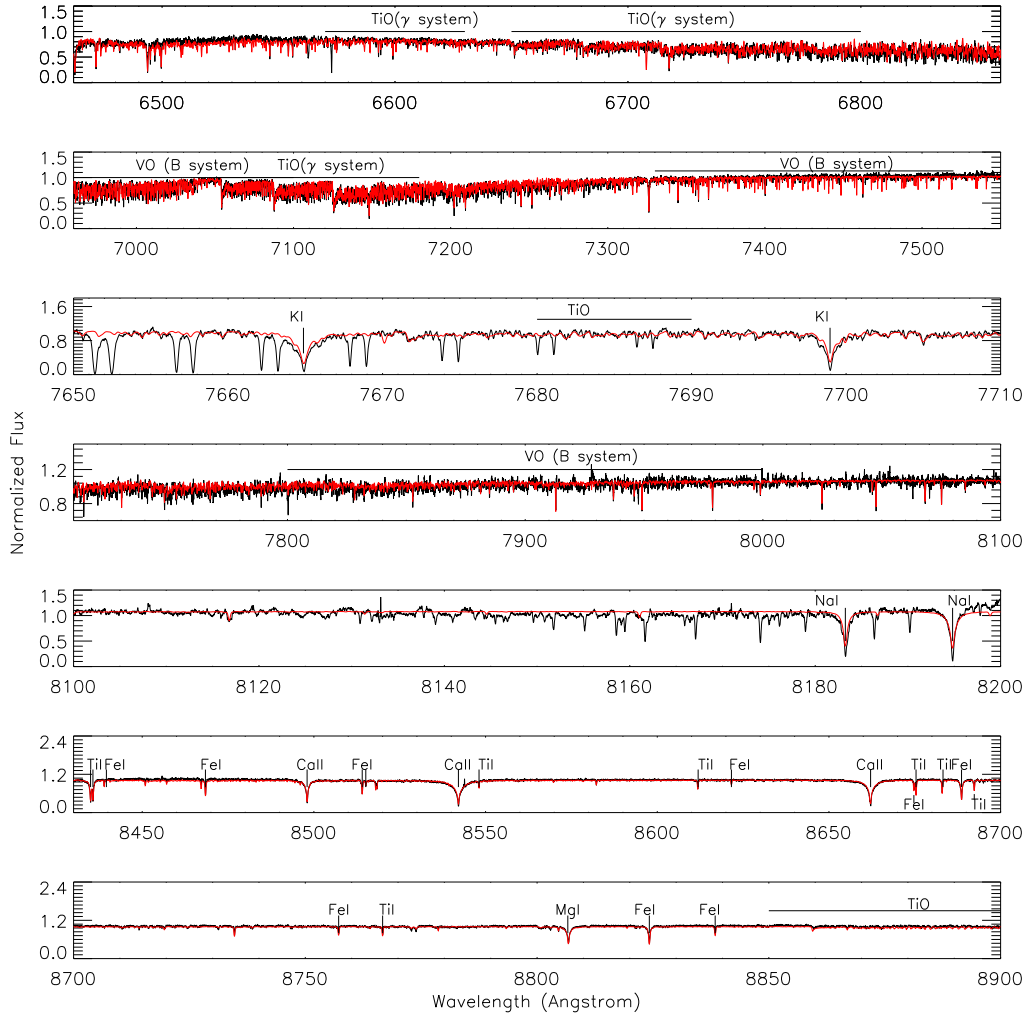


Fig. 4: UVES spectra of the sdM1 star LHS 158 (black) compared to the best fit BT-Settl synthetic spectra (red).

Å and 8194 Å are particular useful gravity discriminants for M dwarfs and subdwarfs. The overall line strength (central depth and equivalent width) increases with gravity as the decreasing ionization ratio due to higher electron pressure leaves more neutral alkali lines in the deeper atmosphere (Reiners 2005). The width of the damping wings in addition increases due to the stronger pressure broadening, mainly by H₂, He and H I collisions.

We also check the metallicity determination on the spectral interval from 8440 Å to 8900 Å where molecular absorptions are less and atomic lines appear clearly (see Fig. 7). The synthetic spectrum give a fairly well representation of the line profiles for elemental species such as Ti, I Fe I, Ca II, and Mg I. The best fit parameters (T_{eff} , $\log g$, [Fe/H]) are given in Table 2.

5. Discussion

The effective temperature versus near-infrared colours are shown in Fig. 8. The expected relations from evolution models (Baraffe et al. 1997, 1998) assuming an age of 10 Gyrs, and varying metallicities, are also superimposed. The colours stand for different metallicities. The plot shows discrepancies between the models and our observations. It shows that the metallicities determined from the high resolution spectral features are incon-

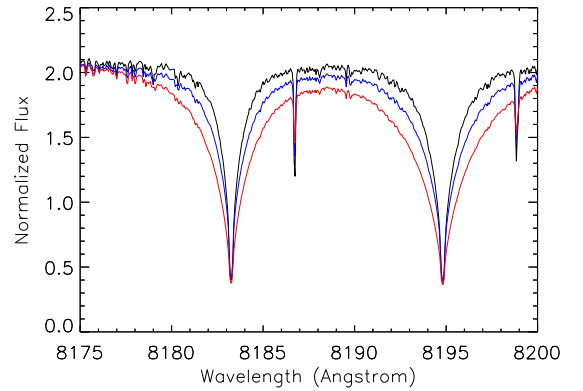


Fig. 6: BT-Settl synthetic spectra with T_{eff} of 3500 K and varying $\log g = 4.5$ (black), 5.0 (blue), 5.5 (red). The effect of gravity and pressure broadening on the sodium doublet is clearly visible.

sistent with those we would infer from near-infrared colours. This inconsistency may be due to uncertainties in the CIA opacities or due to outdated model interiors. It shows that broad band colours are not sufficient to determine the parameters of M subdwarfs.

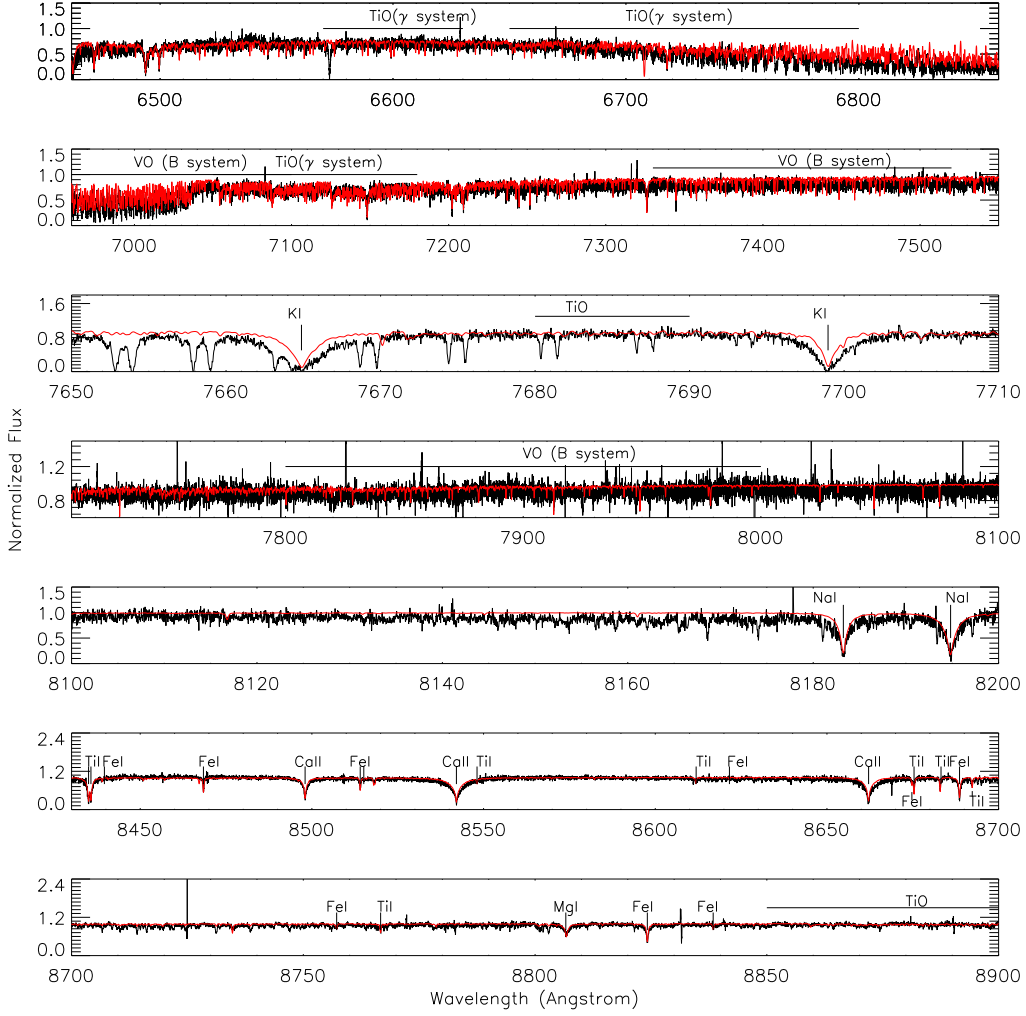


Fig. 5: Same as Fig. 4 for the usdM4.5 star LHS 1032.

The effective temperature versus spectral type relation is shown in Fig. 9. The relation determined using UVES sample is compared to the T_{eff} scale of M dwarfs determined by Rajpurohit et al. (2013). T_{eff} of subdwarfs dwarfs is 200-300 K higher than T_{eff} of M dwarfs for the same spectral type except for hot temperature. This is expected since the TiO bands are depleted with decreasing metallicity, and as a result the pseudo-continuum is brighter and the flux is emitted from the hot deeper layer. A comparison to the earlier work from Gizis (1997) is also shown. Gizis (1997) determined the temperature by comparing the low resolution optical spectra of a sample of sdM and esdM with the NextGen model atmosphere grid by Allard et al. (1997). The T_{eff} for subdwarfs are in agreement within 100 K. This difference is due to the incompleteness of the TiO and water vapor line lists used in the NextGen model atmospheres compared to the new BT-Settl models. Furthermore this work allows us to extend the relation to the coolest M subdwarfs.

We compile from the literature the spectral indices TiO5, CaH2, and CaH3, computed from TiO and CaH band strengths on low resolution spectra (see Table 1). The last column gives the references for spectral types and spectral indices. When possible, we take both the spectral type and the indices from the same paper. We note that the spectral indices may vary over several subtypes for some of the stars from one author to the other. Since Jao et al. (2008) do not give new spectral types in the scheme

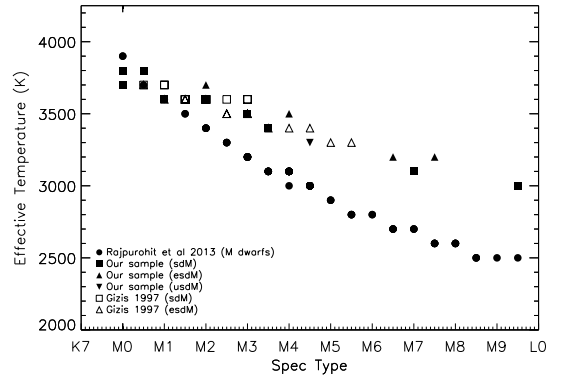


Fig. 9: Effective temperature of subdwarfs versus spectral type relation from our sample (filled symbols) compared to the one from Gizis (1997) (open symbols) and to the M dwarfs T_{eff} scale from Rajpurohit et al. (2013) (filled circles).

developed by Gizis (1997) and extended by Lépine et al. (2007) (sd, esd, usd) that we chose to use in this paper, we adopt the indices from Jao et al. (2008) and assign sdM types only in those

Table 2: Stellar Parameters of the observed targets.

Target	Spectral Type	T_{eff}	$\log g$	[Fe/H]
LHS 72	sdK4	3900 ± 23	4.5 ± 0.13	-1.4 ± 0.27
LHS 73	sdK7	3800 ± 39	4.5 ± 0.13	-1.4 ± 0.19
G 18-37	esdK7	3800 ± 78	4.5 ± 0.15	-1.3 ± 0.44
APMPM J2126-4454	sdM0	3700 ± 49	4.5 ± 0.19	-1.3 ± 0.23
LHS 300	sdM0	3800 ± 39	4.5 ± 0.17	-1.4 ± 0.24
LHS 401	sdM0.5	3800 ± 26	4.5 ± 0.17	-1.4 ± 0.28
LHS 158	sdM1	3600 ± 48	4.5 ± 0.17	-1.0 ± 0.3
LHS 320	sdM2	3600 ± 59	4.6 ± 0.23	-0.6 ± 0.31
LHS 406	sdM2	3600 ± 40	4.7 ± 0.24	-0.6 ± 0.24
LHS 161	esdM2 ^a	3700 ± 77	4.8 ± 0.30	-1.2 ± 0.36
LP 771-87	usdM2	3600 ± 95	4.8 ± 0.31	-1.4 ± 0.52
LHS 541	sdM3	3500 ± 76	5.1 ± 0.31	-1.0 ± 0.39
LHS 272	sdM3	3500 ± 66	5.2 ± 0.30	-0.7 ± 0.37
LP 707-15	esdM3	3500 ± 68	5.5 ± 0.29	-0.5 ± 0.36
LSR J1755+1648	sdM3.5	3400 ± 52	5.1 ± 0.31	-0.5 ± 0.33
LHS 375	esdM4	3500 ± 79	5.5 ± 0.32	-1.1 ± 0.31
LHS 1032	usdM4.5	3300 ± 63	4.5 ± 0.32	-1.7 ± 0.25
SSSPM J0500-5406	esdM6.5	3200 ± 51	5.4 ± 0.31	-1.6 ± 0.16
LHS 377	sdM7	3100 ± 32	5.3 ± 0.25	-1.0 ± 0.16
APMPM J0559-2903	esdM7	3200 ± 68	5.4 ± 0.34	-1.7 ± 0.25
SSPM J1013-1356	sdM9.5	3000 ± 0	5.5 ± 0.05	-1.1 ± 0.16

^a The spectral type derived from Gizis (1997) is probably too late due to an observational problem that affects the extreme red slope of the spectrum (J. Gizis, private communication). This is in agreement with the warmer temperature we derived for this object.

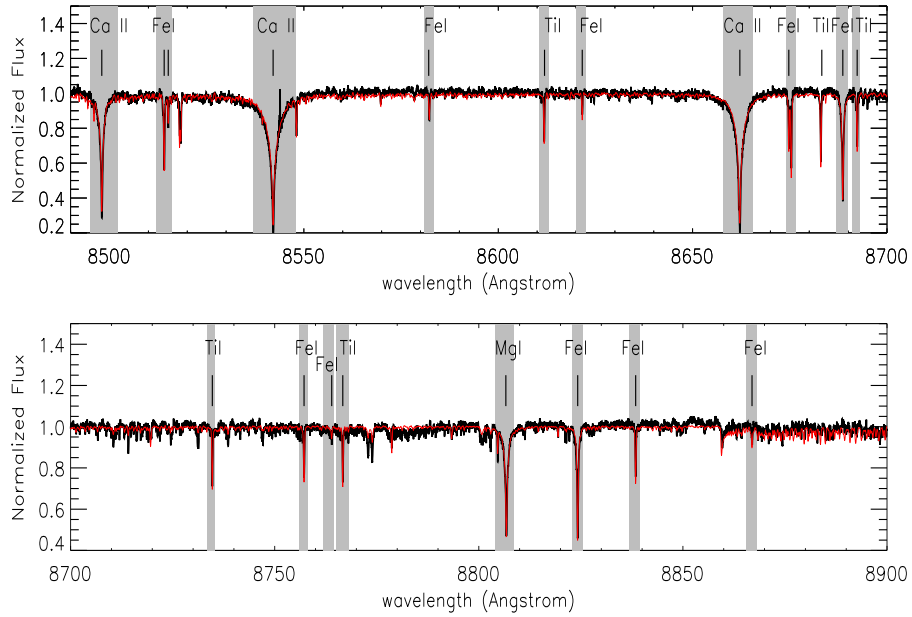


Fig. 7: UVES spectrum of the sdM1 star LHS 158 (black) and the best fit BT Settl synthetic spectrum (red). The strong atomic features are highlighted.

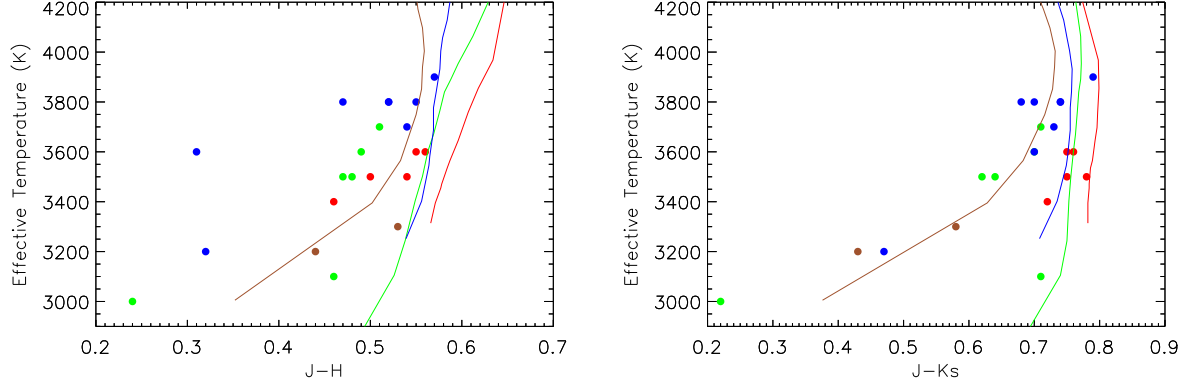


Fig. 8: Effective temperature versus near infrared colours of our sample of subdwarfs. The different colours stand for different metallicities: $[\text{Fe}/\text{H}] = -0.5$ to -0.7 dex (red), $[\text{Fe}/\text{H}] = -1.0$ to -1.2 dex (green), $[\text{Fe}/\text{H}] = -1.3$ to -1.6 dex (blue), $[\text{Fe}/\text{H}] = -1.7$ dex (brown). The lines are from evolution models from (Baraffe et al. 1998) at different metallicities (red: -0.5 dex, green: -1.0 dex, blue: -1.5 dex, brown: -2.0 dex) assuming an age of 10 Gyr.

cases where no indices are available from the papers providing an sd, esd, usd classification.

Fig 10 shows the CaH2+CaH3 versus TiO5. Lépine et al. (2003b) showed that such a diagram is useful to discriminate between the different object classes, sdM, esdM, and usdM. Our metallicity determinations are labelled in the diagram. It shows that the metallicity is, as expected, getting lower from sdM to usdM stars.

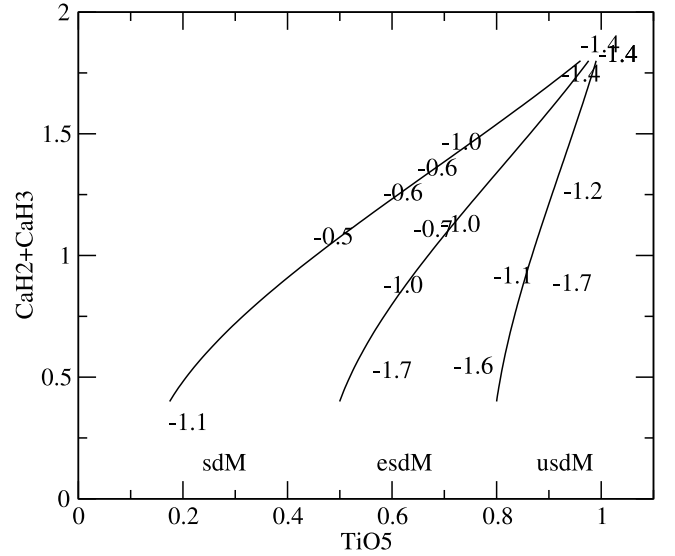


Fig. 10: CaH2+CaH3 versus TiO5 diagram for our sample. The labels indicate our metallicity determination. The lines are defined by Lépine et al. (2007). They show the different regions in the diagram where sdM, esdM, and usdM stars are expected to be.

We also derive the ζ parameter as defined by Lépine et al. (2007). This ζ parameter is a combination of the TiO5, CaH2 and CaH3 spectral indices. Woolf et al. (2009) used a sample of 12 esdM and usdM with known metallicity to derive a correlation between ζ and the metallicity, and showed that it can be used as a metallicity indicator. We plot the metallicity of our stars versus ζ

(Fig. 11) and superimposed the sample from Woolf et al. (2009) as well as their derived correlation (dashed line). We also define a similar correlation (solid line) using our sample

$$[Fe/H] = 1.19\zeta - 1.75$$

Although the relation shows a strong dispersion in both sample, our metallicity determinations tend to be lower on average. This can be due to different spectral indices adopted, or to the use of different atmosphere models. LHS 161, the only common star in both sample, illustrates the first assumption. Our metallicity determination (-1.2 dex) is in agreement with that of Woolf et al. (2009) (-1.3 dex) but the spectral indices adopted are very different: we use $\zeta = 0.07$ from Gizis (1997) indices whereas Woolf et al. (2009) used $\zeta = 0.41$ from Jao et al. (2008) indices. Furthermore, Woolf et al. (2009) used NextGen models.

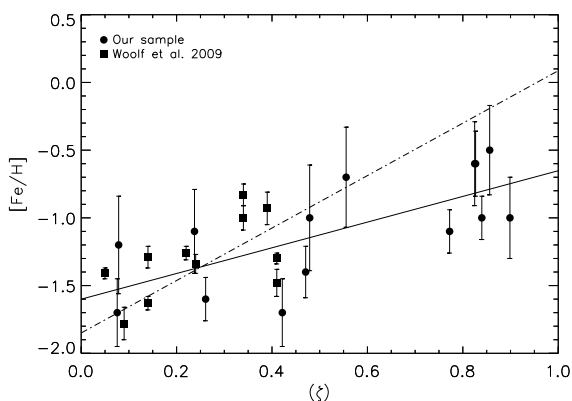


Fig. 11: ζ parameter defined by Lépine et al. (2007) versus metallicity diagram. The circles show our sample and the solid black line is the linear-square regression. The sample from Woolf et al. (2009) is superimposed (squares) as well as their derived relation (dashed line).

6. Conclusion

We present a high resolution optical spectral atlas for a sample of 18 M subdwarfs and 3 K subdwarfs, including 5/1 esdK/esdM and 2 usdM³. We describe various atomic and molecular features that appear in the spectra and their evolution with decreasing effective temperature and metallicity. We use the most recent BT-Settl model atmospheres, with revised solar abundances, to determine the scaled solar abundances of the subdwarfs. We compare them with the synthetic spectra produced by the BT-Settl atmosphere models and derive their fundamental stellar parameters. The accuracy of the atmospheric models involved in the metallicity determination can be inferred by looking at the fit to the individual atomic and molecular lines. Working with these high resolution spectra allowed us to disentangle the atmospheric parameters (effective temperature, gravity, metallicity), which is not possible when using broad-band photometry.

We determine an effective temperature versus spectral type relation of M-subdwarfs and compare it to the previous study from Gizis (1997). Our relation is in agreement within 100 K, and extend to the cooler spectral sequence. This work also contributes towards calibrating the relation between metallicity and photometric colours and molecular band strengths. With such a

calibration, it will be possible to estimate the metallicity of large sample of subdwarfs, allowing meaningful statistical analysis to be performed.

The next step of this work is to investigate the effect of different alpha enhancement on the spectral energy distribution and the spectral line strengths of M subdwarfs. This effect is expected to be as important as the revised oxygen abundances were to make the models fit solar metallicity M dwarfs. This is a limitation of the models since M subdwarfs are actually spread into two regimes, each with rough prescription of alpha enhancement. More realistic abundance trends should be applied to the models (Neves et al. 2009; Adibekyan et al. 2012). This atlas is appropriate to test these prescriptions their effect on the atmosphere spectra as they are precise enough to allow us to derive elemental abundances.

Acknowledgements. We acknowledge observing support from the ESO staff. We acknowledge financial support from "Programme National de Physique Stellaire" (PNPS) (CNRS/INSU, France). We thank the referee J. Gizis for his useful comments on the paper.

References

- Abel, M., Frommhold, L., Li, X., & Hunt, K. L. C. 2011, in 66th International Symposium On Molecular Spectroscopy
- Adibekyan, V. Z., Sousa, S. G., Santos, N. C., et al. 2012, A&A, 545, A32
- Allard, F. 1990, PhD thesis, PhD thesis. Ruprecht Karls Univ. Heidelberg, (1990)
- Allard, F. & Hauschildt, P. H. 1995, ApJ, 445, 433
- Allard, F., Hauschildt, P. H., Alexander, D. R., & Starrfield, S. 1997, ARA&A, 35, 137
- Allard, F., Hauschildt, P. H., Alexander, D. R., Tamanai, A., & Schweitzer, A. 2001, ApJ, 556, 357
- Allard, F., Homeier, D., & Freytag, B. 2012, Royal Society of London Philosophical Transactions Series A, 370, 2765
- Allard, F., Homeier, D., Freytag, B., et al. 2013, Memorie della Societa Astronomica Italiana Supplementi, 24, 128
- Allard, N. F., Kielkopf, J. F., & Allard, F. 2007, European Physical Journal D, 44, 507
- Alloin, D. & Bica, E. 1989, A&A, 217, 57
- Asplund, M., Grevesse, N., Sauval, A. J., & Scott, P. 2009, ARA&A, 47, 481
- Bailey, J. & Kedziora-Chudczer, L. 2012, MNRAS, 419, 1913
- Baraffe, I., Chabrier, G., Allard, F., & Hauschildt, P. H. 1997, A&A, 327, 1054
- Baraffe, I., Chabrier, G., Allard, F., & Hauschildt, P. H. 1998, A&A, 337, 403
- Barber, R. J., Tennyson, J., Harris, G. J., & Tolchenov, R. N. 2006, MNRAS, 368, 1087
- Barklem, P. S., Piskunov, N., & O'Mara, B. J. 2000, A&A, 363, 1091
- Bean, J. L., Sneden, C., Hauschildt, P. H., Johns-Krull, C. M., & Benedict, G. F. 2006a, ApJ, 652, 1604
- Bean, J. L., Sneden, C., Hauschildt, P. H., Johns-Krull, C. M., & Benedict, G. F. 2006b, ApJ, 652, 1604
- Bidelman, W. P. 1985, ApJS, 59, 197
- Bonfils, X., Forveille, T., Delfosse, X., et al. 2005, A&A, 443, L15
- Borysow, A. & Frommhold, L. 1989, ApJ, 341, 549
- Borysow, A., Jørgensen, U. G., & Fu, Y. 2001, Journal of Quantitative Spectroscopy and Radiative Transfer, 68, 235
- Borysow, A., Jørgensen, U. G., & Zheng, C. 1997, A&A, 324, 185
- Burgasser, A. J. & Kirkpatrick, J. D. 2006, ApJ, 645, 1485
- Burgasser, A. J., Kirkpatrick, J. D., Burrows, A., et al. 2003, ApJ, 592, 1186
- Caffau, E., Ludwig, H.-G., Steffen, M., Freytag, B., & Bonifacio, P. 2011, Sol. Phys., 268, 255
- Casagrande, L., Flynn, C., & Bessell, M. 2008, MNRAS, 389, 585
- Chowdhury, P. K., Merer, A. J., Rixon, S. J., Bernath, P. F., & Ram, R. S. 2006, Physical Chemistry Chemical Physics (Incorporating Faraday Transactions), 8, 822
- Dawson, P. C. & De Robertis, M. M. 2000, AJ, 120, 1532
- Deen, C. P. 2013, AJ, 146, 51
- Dekker, H., D'Odorico, S., Kaufer, A., Delabre, B., & Kotzlowski, H. 2000, in Society of Photo-Optical Instrumentation Engineers (SPIE) Conference Series, Vol. 4008, Society of Photo-Optical Instrumentation Engineers (SPIE) Conference Series, ed. M. Iye & A. F. Moorwood, 534-545
- Digby, A. P., Hambly, N. C., Cooke, J. A., Reid, I. N., & Cannon, R. D. 2003, MNRAS, 344, 583
- Dulick, M., Bauschlicher, Jr., C. W., Burrows, A., et al. 2003, ApJ, 594, 651
- Freytag, B., Steffen, M., Ludwig, H.-G., et al. 2012, J. Comp. Phys., 231, 919

³ The atlas will be made public through the Virtual Observatory tools.

- Gamache, R. R., Lynch, R., & Brown, L. R. 1996, *J. Quant. Spec. Radiat. Transf.*, 56, 471
- Gizis, J. E. 1997, *AJ*, 113, 806
- Goorvitch, D. & Chackarian, Jr., C. 1994a, *ApJS*, 91, 483
- Goorvitch, D. & Chackarian, Jr., C. 1994b, *ApJS*, 92, 311
- Gustafsson, B., Edvardsson, B., Eriksson, K., et al. 2008, *A&A*, 486, 951
- Gustafsson, M. & Frommhold, L. 2001, *ApJ*, 546, 1168
- Gustafsson, M., Kristensen, L. E., Cl  net, Y., et al. 2003, *A&A*, 411, 437
- Hauschildt, P. H., Baron, E., & Allard, F. 1997, *ApJ*, 483, 390
- Jao, W.-C., Henry, T. J., Beaulieu, T. D., & Subasavage, J. P. 2008, *AJ*, 136, 840
- Johnas, C. M. S., Hauschildt, P. H., Schweitzer, A., et al. 2007, *A&A*, 475, 1039
- Kirkpatrick, J. D., Looper, D. L., Burgasser, A. J., et al. 2010, *ApJS*, 190, 100
- L  pine, S., Rich, R. M., & Shara, M. M. 2003a, *AJ*, 125, 1598
- L  pine, S., Rich, R. M., & Shara, M. M. 2007, *ApJ*, 669, 1235
- L  pine, S., Shara, M. M., & Rich, R. M. 2003b, *AJ*, 126, 921
- Ludwig, H.-G., Allard, F., & Hauschildt, P. H. 2002, *A&A*, 395, 99
- Ludwig, H.-G., Allard, F., & Hauschildt, P. H. 2006, *A&A*, 459, 599
- Mallik, S. V. 1997, *A&AS*, 124, 359
- Neves, V., Santos, N. C., Sousa, S. G., Correia, A. C. M., & Israelian, G. 2009, *A&A*, 497, 563
-   nehag, A., Heiter, U., Gustafsson, B., et al. 2012, *A&A*, 542, A33
- Plez, B. 1998, *A&A*, 337, 495
- Rajpurohit, A. S., Reyl  , C., Allard, F., et al. 2013, *A&A*, 556, A15
- Rajpurohit, A. S., Reyl  , C., Schultheis, M., et al. 2012, *A&A*, 545, A85
- Reiners, A. 2005, *Astronomische Nachrichten*, 326, 930
- Reiners, A. & Basri, G. 2006, *AJ*, 131, 1806
- Reiners, A., Homeier, D., Hauschildt, P. H., & Allard, F. 2007, *A&A*, 473, 245
- Reyl  , C., Scholz, R.-D., Schultheis, M., Robin, A. C., & Irwin, M. 2006, *MNRAS*, 373, 705
- Rodgers, A. W. & Eggen, O. J. 1974, *PASP*, 86, 742
- Rothman, L. S., Gordon, I. E., Barbe, A., et al. 2009, *J. Quant. Spec. Radiat. Transf.*, 110, 533
- Scholz, R.-D., Ibata, R., Irwin, M., et al. 2002, *MNRAS*, 329, 109
- Scholz, R.-D., Lehmann, I., Matute, I., & Zinnecker, H. 2004, *A&A*, 425, 519
- Schweitzer, A., Scholz, R.-D., Stauffer, J., Irwin, M., & McCaughrean, M. J. 1999, *A&A*, 350, L62
- Skory, S., Weck, P. F., Stancil, P. C., & Kirby, K. 2003, *ApJS*, 148, 599
- Skrutskie, M. F., Cutri, R. M., Stiening, R., et al. 2006, *AJ*, 131, 1163
- Tashkun, S. A., Perevalov, V. I., Teffo, J.-L., et al. 2004, *Proc. SPIE*, 5311, 102
- Tinney, C. G. & Reid, I. N. 1998, *MNRAS*, 301, 1031
- Unsold, A. 1968, *Physik der Sternatmosph  ren*, MIT besonder Berucksichtigung der Sonne
- Valenti, J. A. & Piskunov, N. 1996, *A&AS*, 118, 595
- Weck, P. F., Schweitzer, A., Stancil, P. C., Hauschildt, P. H., & Kirby, K. 2003, *ApJ*, 584, 459
- Woolf, V. M., L  pine, S., & Wallerstein, G. 2009, *PASP*, 121, 117
- Woolf, V. M. & Wallerstein, G. 2005, *MNRAS*, 356, 963
- Zhou, X. 1991, *A&A*, 248, 367